

Article

Structure and Properties of Ln_2MoO_6 Oxymolybdates ($Ln = La, Pr, Nd$) Doped with Magnesium

Ekaterina Orlova ¹, Elena Kharitonova ¹, Timofei Sorokin ², Alexander Antipin ², Nataliya Novikova ² , Nataliya Sorokina ²  and Valentina Voronkova ^{1,*}

¹ Faculty of Physics, Moscow State University, Moscow 119991, Russia; agapova@polly.phys.msu.ru (E.O.); harit@polly.phys.msu.ru (E.K.)

² Shubnikov Institute of Crystallography, Federal Scientific Research Centre “Crystallography and Photonics”, Russian Academy of Sciences, Moscow 119333, Russia; tim29@inbox.ru (T.S.); antipin@physics.msu.ru (A.A.); nata110565@mail.ru (N.N.); nsor@ns.crys.ras.ru (N.S.)

* Correspondence: voronk@polly.phys.msu.ru; Tel.: +7-495-939-28-83

Abstract: The literature data and the results obtained by the authors on the study of the structure and properties of a series of polycrystalline and single-crystal samples of pure and Mg-doped oxymolybdates Ln_2MoO_6 ($Ln = La, Pr, Nd$) are analyzed. Presumably, the high-temperature phase $I4_1/acd$ of Nd_2MoO_6 single crystals is retained at room temperature. The reason for the loss of the center of symmetry in the structures of La_2MoO_6 and Pr_2MoO_6 and the transition to the space group $\bar{1}4c2$ is the displacement of oxygen atoms along the twofold diagonal axes. In all structures, Mg cations are localized near the positions of the Mo atoms, and the splitting of the positions of the atoms of rare-earth elements is found. Thermogravimetric studies, as well as infrared spectroscopy data for hydrated samples of Ln_2MoO_6 ($Ln = La, Pr, Nd$), pure and with an impurity of Mg, confirm their hygroscopic properties.

Keywords: oxymolybdates; rare-earth elements; crystal structure; X-ray diffraction; growth from flux; solid-state reactions; thermogravimetry; infrared spectroscopy



Citation: Orlova, E.; Kharitonova, E.; Sorokin, T.; Antipin, A.; Novikova, N.; Sorokina, N.; Voronkova, V. Structure and Properties of Ln_2MoO_6 Oxymolybdates ($Ln = La, Pr, Nd$) Doped with Magnesium. *Crystals* **2021**, *11*, 611. <https://doi.org/10.3390/cryst11060611>

Academic Editor: Daniel Errandonea

Received: 6 May 2021

Accepted: 26 May 2021

Published: 28 May 2021

Publisher's Note: MDPI stays neutral with regard to jurisdictional claims in published maps and institutional affiliations.



Copyright: © 2021 by the authors. Licensee MDPI, Basel, Switzerland. This article is an open access article distributed under the terms and conditions of the Creative Commons Attribution (CC BY) license (<https://creativecommons.org/licenses/by/4.0/>).

1. Introduction

During decades, tungstates, molybdates, and binary systems of the Ln_2O_3 – $Mo(W)O_3$ type, especially in the concentration range 25–50 mol% of Ln_2O_3 oxide, have been intensively studied [1–6]. The different content of oxides determines the variety of compounds in these systems. Scheelite-like 1:3 phases (the 1:3 ratio of molar concentrations of oxides, i.e., the 1:3 composition) with excellent luminescent properties are distinguished among them. In the molybdates of these compounds, improper ferroelectrics were first discovered [7]. In 2000, the LAMOX family (1:2 composition) with a high oxygen conductivity of the order of 10^{-2} S cm^{-1} was discovered [8]. The cubic phase of the 5:6 composition ($Ln_5Mo_3O_{16}$) [9] has the same high conductivity. Finally, 1:1 compounds ($Ln_2Mo(W)O_6$), so-called oxymolybdates and oxytungstates, existing in all the binary systems mentioned above, exhibit polymorphism that depends on the ionic radius of the rare earth element and the synthesis temperature [1–6]. Oxymolybdates and oxytungstates are chemically stable and have high refractive indices. These compounds doped with Eu exhibit intense luminescence [10,11] and are also used as microwave ceramics [12,13]. Other properties of these compounds are poorly understood. Let us focus our attention on the study of a number of new properties of the rather well-studied phases of oxymolybdates and oxytungstates $Ln_2Mo(W)O_6$ existing in binary systems Ln_2O_3 – $Mo(W)O_3$ [1,4,14–17].

Already in the first and subsequent structural studies, polymorphism in these compounds was revealed [1,2,4,14–20]. Oxytungstates were synthesized in two different monoclinic scheelite-like symmetry classes, depending on the ionic radius of the rare earth element [1]. As for oxymolybdates Ln_2MoO_6 with large rare earth cations (La, Pr, and Nd),

a large number of works have been devoted to the study of their polymorphism, structure, and properties [14–17,19]. During the synthesis of these oxymolybdates at a temperature of about 1200 °C, a layered tetragonal phase is formed. With a subsequent decrease in the ionic radius, a monoclinic scheelite-like phase with a structure of the Nd_2WO_6 type was synthesized, which remained monoclinic when heated to 1400 °C [1,2,4,15]. Scheelite-like structures of the Nd_2WO_6 -type for oxymolybdates Ln_2MoO_6 ($\text{Ln} = \text{Nd–Tb}$) have been studied many times [15,17,19]. Among Ln_2MoO_6 molybdates with large cations ($\text{Ln} = \text{La–Nd}$), only Nd_2MoO_6 can exist at low temperatures in the monoclinic phase, which irreversibly transforms into the tetragonal phase at 1010 °C [21]. The existence of this phase transition was confirmed by differential thermal analysis (DTA).

In [14], the structure of La_2MoO_6 single crystals obtained at 800 °C was studied for the first time. The authors revealed their tetragonal layered structure, space group $\bar{I}4_2m$, and unit cell parameters $a = 4.089$, $c = 15.99$ Å. No monoclinic phase was found.

According to [16,17], the space group of Ln_2MoO_6 ($\text{Ln} = \text{La, Nd}$) single crystals obtained by cooling from 1250 to 900 °C is centrosymmetric $I4_1/acd$ with a doubled parameter c ($a = 5.798$, $c = 32.036$ Å). This conclusion was first made in [16] and was associated with additional reflections arising from the deformation of the crystal lattice during firing at high temperatures. Further investigation of the physical properties of the crystals revealed a weak piezoelectric effect [16], which made it necessary to reconsider the crystal symmetry. For crystals at room temperature, an asymmetric space group $\bar{I}4c2$ was chosen, which is a subgroup of the space group $I4_1/acd$. The authors of [16] assumed the existence of a second order phase transition between these groups, which was therefore not detected using DTA [22]. According to [16,17], the structure of La_2MoO_6 or Nd_2MoO_6 consists of two layers of LaO_8 or NdO_8 polyhedra and a layer of isolated MoO_4 tetrahedra. The conductivity of oxymolybdates does not exceed 10^{-4} S cm^{-1} [23]. Thermogravimetry shows that molybdates Ln_2MoO_6 ($\text{Ln} = \text{La, Pr, Nd}$) have hygroscopic properties up to 1000–1200 °C, which may indicate the possible proton conductivity in these compounds [24–26].

Currently, a number of works are known in which the rare earth element in oxymolybdates with large cations is partially replaced by divalent elements—lead or magnesium [21,24–26]. Solid solutions $(\text{PbO})_x(\text{Nd}_2\text{MoO}_6)_{(1-x)/2}$ are formed in a wide range $0 \leq x \leq 0.6$. In these solid solutions, in the region of 820 °C, a phase transition was observed between the low-temperature $\bar{I}4_2m$ and high-temperature $I4_1/acd$ phases upon heating. In the phase transition region, the conductivity of neodymium oxymolybdate increased by two orders of magnitude and reached 10^{-2} S cm^{-1} and was comparable to the conductivity of molybdate with the LAMOX structure. When lanthanum oxymolybdate was doped with Pb, the field of solid solutions narrowed [27]. However, the physical properties changed upon doping in the same way as in the case of neodymium oxymolybdate: a phase transition occurred (775 °C), the conductivity increased.

The second divalent element, magnesium, during the synthesis of solid solutions according to the scheme $(\text{MgO})_x(\text{Ln}_2\text{MoO}_6)_{(1-x)/2}$, where $\text{Ln} = \text{La, Pr, Nd}$ [24–26], led to the formation of a very narrow field of solid solutions with $x < 0.10$. Mg-doped single crystals were prepared by flux growth. According to the X-ray diffraction study of the compounds obtained, the Mg atom replaces Mo and leads to the splitting of the positions of rare earth elements, while the phase transition does not occur. In [24–26], the features of the structure and properties of Mg-doped oxymolybdates are considered. The presented work is a brief review in which we summarize, analyze and compare the structural features and properties of Mg-doped Ln_2MoO_6 oxymolybdates with large rare earth cations ($\text{Ln} = \text{La, Pr, Nd}$), previously published and supplemented by studies of a number of new properties using powder X-ray diffraction, thermogravimetry, and infrared spectroscopy.

2. Materials and Methods

Polycrystalline samples were prepared by solid-state reactions in air in ternary systems $\text{MgO–Ln}_2\text{O}_3\text{–MoO}_3$ ($\text{Ln} = \text{La, Pr, Nd}$) in accordance with the scheme $(\text{MgO})_x(\text{Ln}_2\text{O}_3)_y(\text{MoO}_3)_z$

(x , y , z are the molar fractions of oxides, $x + y + z = 1$, $y = z = (1 - x)/2$). These compositions correspond to the Ln_2MoO_6 –MgO binary join of the above ternary system, $(MgO)_x(Ln_2MoO_6)_{(1-x)/2}$, $x = 0, 0.03, 0.05, 0.10$. High purity (99.9%) reagents of magnesium oxide MgO and rare earth oxides La_2O_3 , Pr_2O_3 , and Nd_2O_3 , due to their hygroscopicity, were preliminarily dried before weighing. The tablets of the required composition were compressed using a hydraulic press (10 MPa). Two-stage firing of specimens at temperatures of 800 and 1250 °C for 24 h with intermediate grinding in an agate mortar was applied. The heating and cooling rate was 300 °C h^{−1}.

The surface of the samples of pure and Mg-doped Pr_2MoO_6 was studied by scanning electron microscopy (SEM) using a Scios DualBeam system (scanning electron microscope (SEM)/focus ion beam) (Thermo Fisher Scientific, Waltham, MA, USA). The samples were mounted on an aluminum holder with carbon adhesive tape. SEM image of pure Pr_2MoO_6 ceramics shows weakly faceted crystallites up to 5 μm in size (Figure 1a). The incorporation of Mg into ceramics (Figure 1b) led to an increase in the crystallite size to 10–50 μm and a decrease in the number of pores.

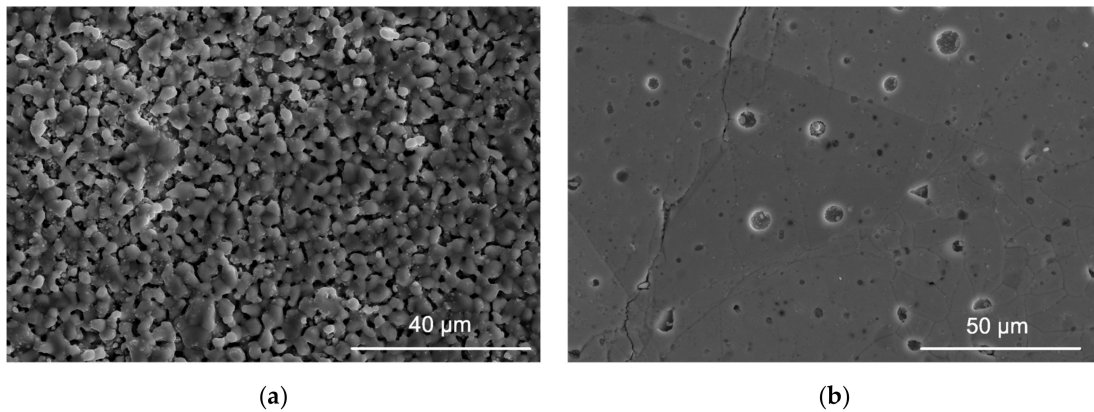


Figure 1. Secondary electron SEM images of: (a) pure; (b) Mg-doped $(MgO)_x(Ln_2MoO_6)_{(1-x)/2}$ ceramics ($x = 0.1$).

Single crystals of rare earth oxymolybdates Ln_2MoO_6 ($Ln = La, Pr, Nd$) were prepared by flux growth in the Li_2O – MoO_3 – Ln_2O_3 , $Ln = La, Pr, Nd$, ternary systems from high-temperature melts with a composition of 12.5 mol% Ln_2O_3 , 30 mol% Li_2O , and 57.5 mol% MoO_3 . To obtain Mg-doped single-crystal samples, magnesium oxide was added to the melt. The maximum melt temperature was 1350 °C. All the obtained single crystals had a plate-like shape, sizes up to 5 mm. Depending on the rare earth cation, the crystals were colorless ($Ln = La$), yellow ($Ln = Pr$), or violet ($Ln = Nd$) in the light of an incandescent lamp (Figure 2a). The good quality of the obtained single crystals was confirmed by SEM. In the SEM image of a Mg-doped Pr_2MoO_6 single crystal, no domains and block boundaries were found (Figure 2b).

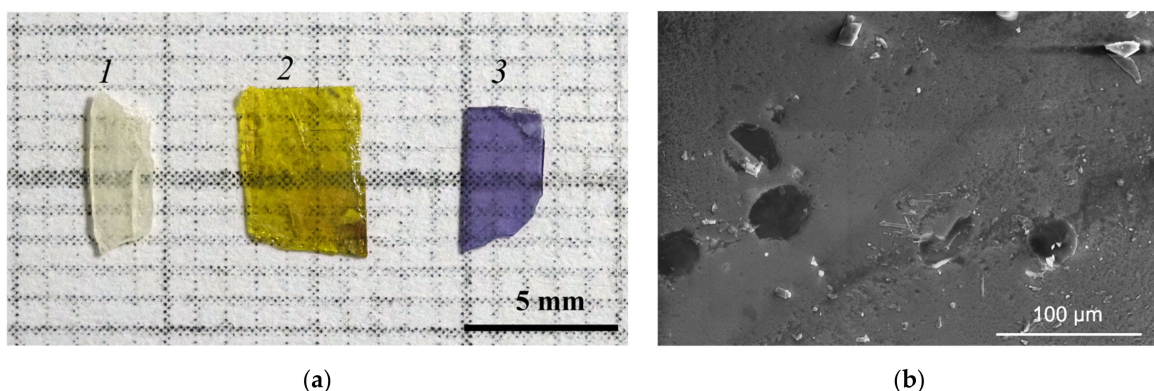


Figure 2. (a) photograph of Mg-containing Ln_2MoO_6 single crystals illuminated by an incandescent lamp: (1) $Ln = La$, (2) Pr , (3) Nd ; (b) secondary electron SEM images of Mg-doped Pr_2MoO_6 single crystal.

The chemical composition of Mg-doped Nd_2MoO_6 and Pr_2MoO_6 was determined in [24,25] using energy dispersive X-ray spectrometry. More precisely, the low concentration of magnesium in Pr_2MoO_6 single crystals was determined by inductively coupled plasma-mass spectrometry (ICP-MS technique) [25].

X-ray phase analysis was carried out at room temperature using a Rigaku Miniflex 600 diffractometer (Cu $K\alpha$ radiation, $2\theta = 20^\circ\text{--}60^\circ$).

To estimate the density of the obtained polycrystalline samples, we used the ratio of the density obtained by hydrostatic weighing in toluene and the X-ray density of the samples, calculated by the formula:

$$\rho_{\text{calc}} = MZ 1.66/V,$$

where M is the molecular weight (g), Z is the number of formula units, V is the volume of the unit cell (\AA^3). The density of pure and Mg-containing polycrystalline samples averaged 95% of the calculated one.

Thermogravimetric (TG) studies of all obtained phases were carried out on NETZSCH STA 449C equipment in the temperature range $20\text{--}1250^\circ\text{C}$ in air at a heating and cooling rate of $10^\circ\text{C min}^{-1}$. Infrared (IR) spectroscopy of the compounds under study was carried out on a Bruker Vertex 70 IR Fourier spectrometer in the frequency range $500\text{--}5000\text{ cm}^{-1}$. A sample of 1.0 mg ground into powder was pressed with potassium bromide into a tablet weighing 200 mg and 0.5 mm thick. Polycrystalline and single-crystal samples for IR and TG studies were preliminarily hydrated by immersion in distilled water at room temperature for one–three weeks.

X-ray diffraction studies of Ln_2MoO_6 ($\text{Ln} = \text{La, Pr, Nd}$) single crystals, pure and doped with Mg, were carried out on an Xcalibur Eos S2 diffractometer (Rigaku Oxford Diffraction) at room temperature. The CrysAlisPro program [28] was used for data reduction. Absorption correction was made analytically, with allowance for the crystal shape and sizes [29], and the JANA2006 program [30] was used to refine the structural model, which was determined with the Superflip program [31] using the charge-flipping algorithm. The experimental data, including the main characteristics of the crystals under study, the results of the refinement of structures, the coordinates, occupancies of positions, and equivalent atomic displacement parameters are given in [24–26].

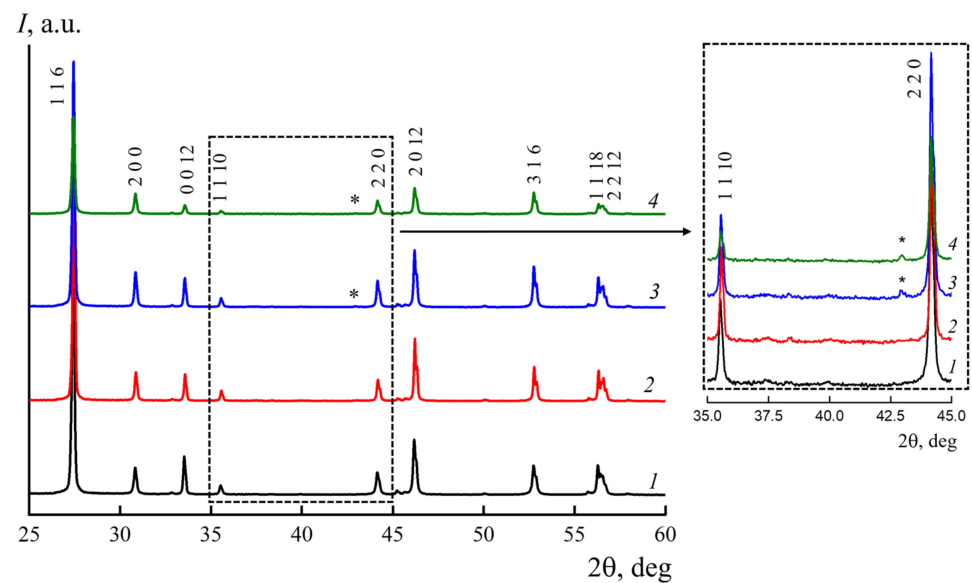
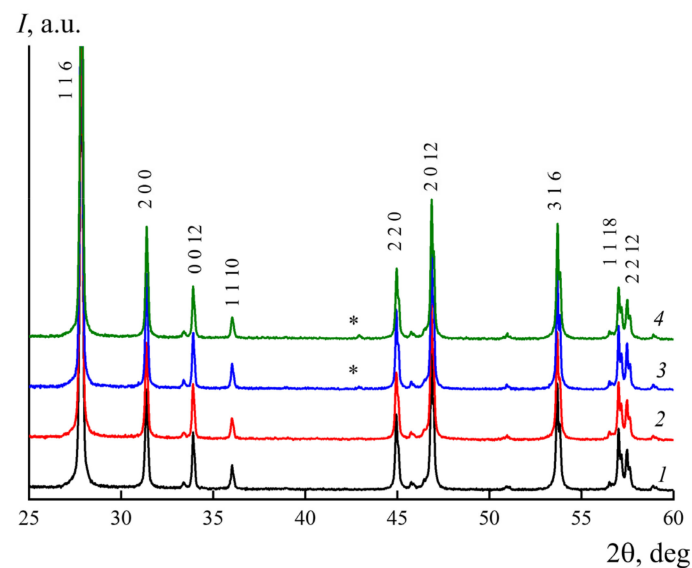
3. Results and Discussion

3.1. Powder X-ray Diffraction

In powder diffraction patterns of ground polycrystalline samples $(\text{MgO})_x(\text{Ln}_2\text{MoO}_6)_{(1-x)/2}$ ($x = 0, 0.03, 0.05, 0.10$), $\text{Ln} = \text{La, Pr}$ (Figures 3 and 4) at $x \geq 0.05$, a peak of a second phase, MgO, emerges ($\theta = 43^\circ$). Samples with $x = 0.03$ are isostructural with pure oxymolybdates La_2MoO_6 and Pr_2MoO_6 . For Mg-containing neodymium oxymolybdates (Figure 5), the solid solution range with a tetragonal structure of Nd_2MoO_6 exists at $x < 0.10$. It should be noted that a wider range of solid solutions is indicated in [24,25] for $(\text{MgO})_x(\text{Ln}_2\text{MoO}_6)_{(1-x)/2}$ ($\text{Ln} = \text{Pr, Nd}$) samples, which is associated with a lower diffractometer resolution. The unit cell parameters of pure and Mg-doped samples of oxymolybdates Ln_2MoO_6 , $\text{Ln} = \text{La, Pr, Nd}$, change insignificantly with the introduction of Mg atoms into the structure of the compounds under study (Table 1).

Table 1. Composition, unit cell parameters and volume of Mg-doped oxymolybdates $(\text{MgO})_x(\text{Ln}_2\text{MoO}_6)_{(1-x)/2}$, $\text{Ln} = \text{La}, \text{Pr}, \text{Nd}$.

Composition	$a, c, \text{\AA}$	$V, \text{\AA}^3$
$(\text{MgO})_x(\text{La}_2\text{MoO}_6)_{(1-x)/2}, x = 0$	5.795(7), 32.054(4)	1076.44(5)
$(\text{MgO})_x(\text{La}_2\text{MoO}_6)_{(1-x)/2}, x = 0.03$	5.791(2), 32.03(1)	1074.15(2)
$(\text{MgO})_x(\text{Pr}_2\text{MoO}_6)_{(1-x)/2}, x = 0$	5.693(9), 31.656(4)	1039.7(9)
$(\text{MgO})_x(\text{Pr}_2\text{MoO}_6)_{(1-x)/2}, x = 0.03$	5.691(1), 31.646(5)	1040.68(0)
$(\text{MgO})_x(\text{Nd}_2\text{MoO}_6)_{(1-x)/2}, x = 0$	5.665(1), 31.638(5)	1015.33(4)
$(\text{MgO})_x(\text{Nd}_2\text{MoO}_6)_{(1-x)/2}, x = 0.03$	5.659(1), 31.622(9)	1012.8(5)
$(\text{MgO})_x(\text{Nd}_2\text{MoO}_6)_{(1-x)/2}, x = 0.05$	5.662(1), 31.616(8)	1013.5(4)

**Figure 3.** Powder X-ray diffraction patterns of ground polycrystalline $(\text{MgO})_x(\text{La}_2\text{MoO}_6)_{(1-x)/2}$ samples: $x = 0$ (1), 0.03 (2), 0.05 (3), 0.10 (4). Asterisks mark the reflections of the MgO impurity phase (inset Figure).**Figure 4.** Powder X-ray diffraction patterns of ground polycrystalline $(\text{MgO})_x(\text{Pr}_2\text{MoO}_6)_{(1-x)/2}$ samples obtained on a Rigaku Miniflex 600 diffractometer: $x = 0$ (1), 0.03 (2), 0.05 (3), 0.10 (4). Asterisks mark the reflections of the MgO impurity phase.

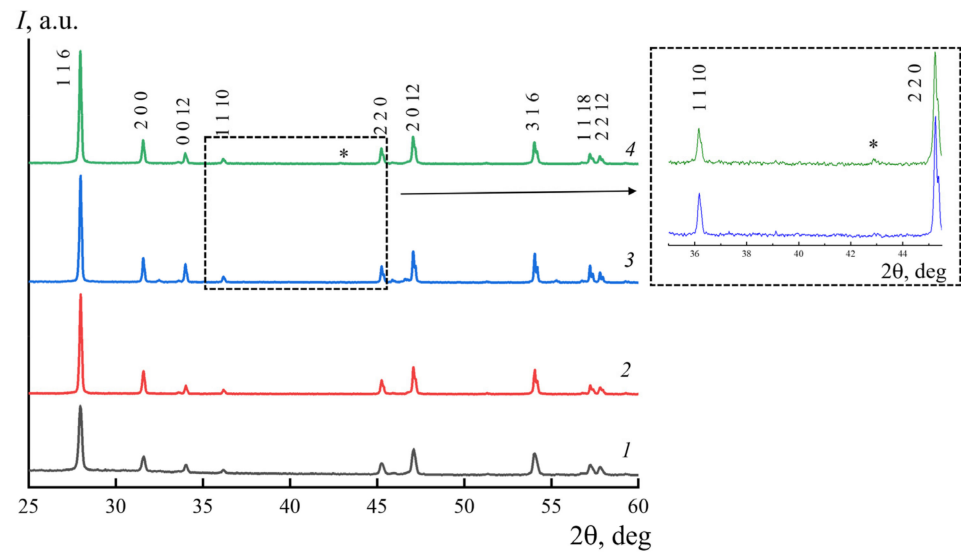


Figure 5. Powder X-ray diffraction patterns of ground polycrystalline $(\text{MgO})_x(\text{Nd}_2\text{MoO}_6)_{(1-x)/2}$ samples obtained on a Rigaku Miniflex 600 diffractometer: $x = 0$ (1), 0.03 (2), 0.05 (3), 0.10 (4). Asterisks mark the reflections of the MgO impurity phase (inset Figure).

Figure 6 shows powder diffraction patterns of ground single crystals of pure and Mg-doped Ln_2MoO_6 , $\text{Ln} = \text{La}, \text{Pr}, \text{Nd}$ [24–26]. There is a significant increase in the intensity of the 0012 reflection in comparison with diffractograms obtained from polycrystalline samples, which is explained by the layered structure of oxymolybdate crystals. The largest face of the crystal is (001) plane (Figure 2a), normal to the c axis.

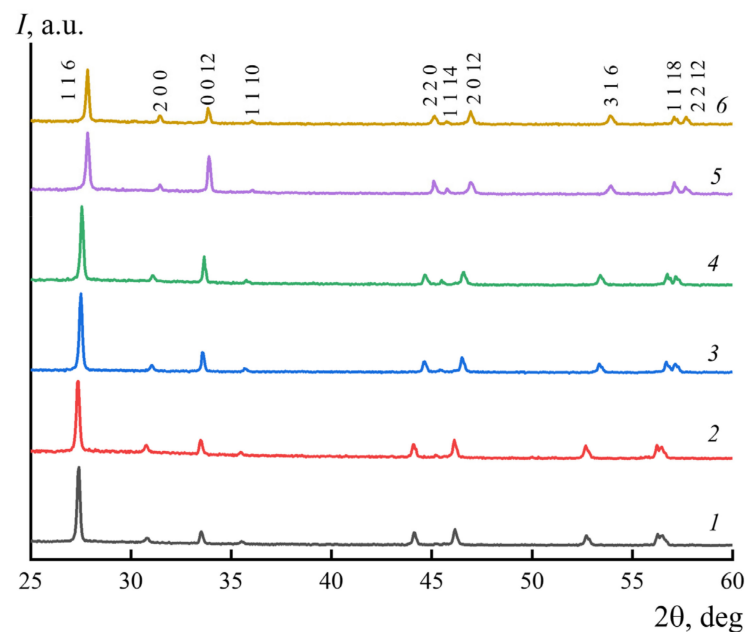


Figure 6. Powder X-ray diffraction patterns of ground single-crystal samples of (1, 3, 5) pure and (2, 4, 6) Mg-containing La_2MoO_6 (1, 2), Pr_2MoO_6 (3, 4), and Nd_2MoO_6 (5, 6).

3.2. Thermogravimetry

In [24–26], the hygroscopic properties of pure and Mg-containing compounds Ln_2MoO_6 ($\text{Ln} = \text{La}, \text{Pr}, \text{Nd}$) were found. In Figures 7 and 8, TG curves of preliminary hydrated polycrystalline and single-crystal Ln_2MoO_6 samples doped with Mg are shown. For all the samples under study, after the first heating, weight losses of the order of 0.1–0.7% were

recorded associated with the evaporation of water. No noticeable weight loss was observed upon reheating, indicating that the water had evaporated. The hygroscopicity of single-crystal samples of La and Nd oxymolybdates was first detected in this work. The weight loss of ceramics and single crystals at high temperatures confirms the presence of water in the crystal structure of the samples [32], not only in the ceramics pores or on the surface.

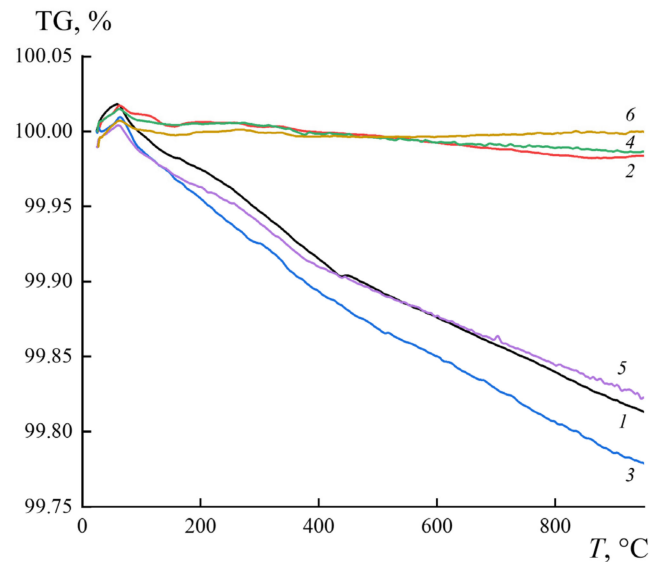


Figure 7. TG curves of (1, 3, 5) hydrated and (2, 4, 6) reheated Mg-containing polycrystalline $(\text{MgO})_{0.03}(\text{La}_2\text{MoO}_6)_{0.485}$ (1, 2), $(\text{MgO})_{0.03}(\text{Pr}_2\text{MoO}_6)_{0.485}$ (3, 4), and $(\text{MgO})_{0.03}(\text{Nd}_2\text{MoO}_6)_{0.485}$ (5, 6) samples.

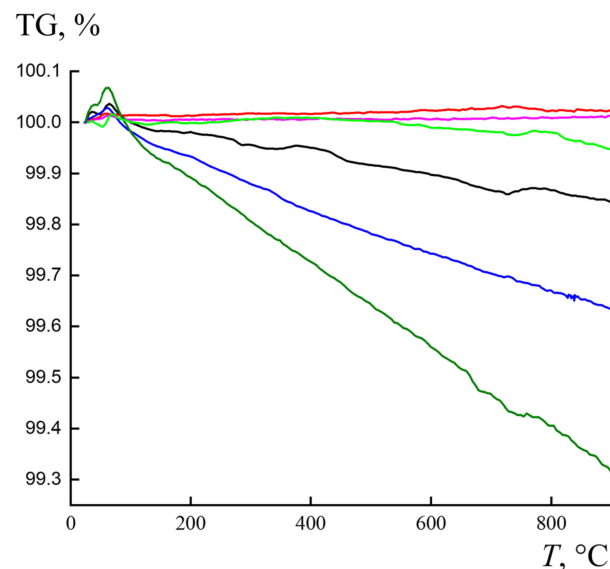


Figure 8. TG curves of (1, 3, 5) hydrated and (2, 4, 6) reheated Mg-containing single crystals La_2MoO_6 (1, 2), Pr_2MoO_6 (3, 4), and Nd_2MoO_6 (5, 6).

The water loss was approximately the same for the ceramics, because ceramics with the same magnesium content were examined ($(\text{MgO})_{0.03}(\text{Ln}_2\text{MoO}_6)_{0.485}$, $\text{Ln} = \text{La}, \text{Pr}, \text{Nd}$) (Figure 7). For single crystals, the amount of absorbed water turned out to be different due to the different concentration of magnesium in the crystals (Figure 8). The largest amount of magnesium was found in neodymium crystals, and the amount of absorbed water for them was the maximum. Apparently, the incorporation of magnesium into the structure increases the hygroscopicity of the samples.

3.3. IR Spectroscopy

IR spectroscopy of Mg-doped polycrystalline oxymolybdate samples is performed for the first time. In Figure 9, the IR spectra of hydrated oxymolybdates $(\text{MgO})_x(\text{Ln}_2\text{MoO}_6)_{(1-x)/2}$, $\text{Ln} = \text{La}, \text{Pr}, \text{Nd}$, $x = 0.03$, are shown. The vibration spectrum of the crystal lattice of the samples under study is recorded below 900 cm^{-1} [33]. Consequently, the region $4500\text{--}900 \text{ cm}^{-1}$ can be attributed to the vibration of OH bonds. For all studied hydrated phases of Mg-containing oxymolybdates, a strong broad band at about 3460 cm^{-1} is observed, which characterizes the stretching vibrations of the O–H bond and confirms the presence of various oxygen-hydrogen groups in the samples. The band corresponding to deformation vibrations of an isolated water molecule shifts to short-wave region and is recorded at 1644 cm^{-1} , which occurs during association of water molecules, for example, due to hydrogen bonds [34,35]. The absorption band at 1730 cm^{-1} unambiguously indicates the existence of the hydroxonium ion H_3O^+ . Thus, it can be concluded that in the studied phases of oxymolybdates, oxygen-hydrogen groups are H_3O^+ .

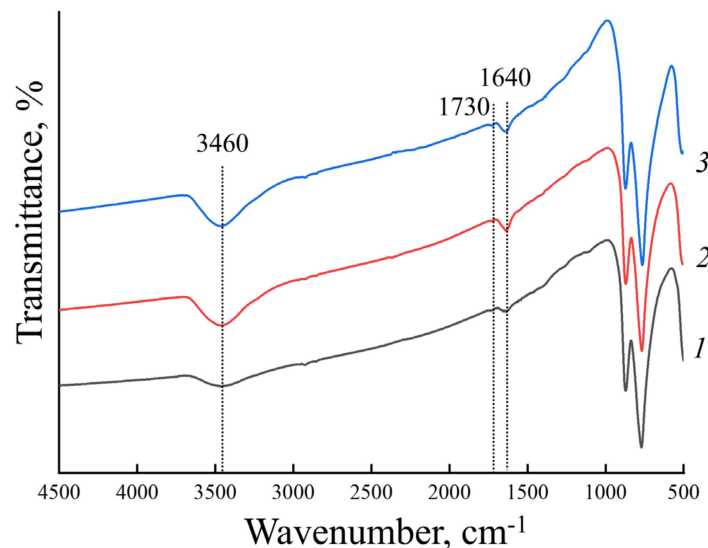


Figure 9. IR spectra of hydrated Mg-containing polycrystalline samples of (1) $\text{La}_2\text{MoO}_6 \cdot n\text{H}_2\text{O}$, (2) $\text{Pr}_2\text{MoO}_6 \cdot n\text{H}_2\text{O}$, and (3) $\text{Nd}_2\text{MoO}_6 \cdot n\text{H}_2\text{O}$.

3.4. Crystal Structure

X-ray diffraction analysis of Mg-doped Ln_2MoO_6 ($\text{Ln} = \text{La}, \text{Pr}, \text{Nd}$) tetragonal single crystals showed that no radical structural changes occurred at an Mg concentration of 2.6–11.4% [24–26]. The structure of these crystals was solved in space group $I4_1/acd$ for Mg-containing samples of neodymium oxymolybdate [24] and in space group $\bar{I}4c2$ for lanthanum and praseodymium oxymolybdates with magnesium [25,26]. The reason for the loss of the center of symmetry and the transition to the space group $\bar{I}4c2$ can be the displacement of O atoms, which form the nearest environment of the atoms of the rare earth elements, along the twofold diagonal axes [16]. Table 2 lists the coordinates of the Ln (La, Pr, Nd), Mo, and O atoms in three structures Ln_2MoO_6 in space groups $I4_1/acd$ and $\bar{I}4c2$, as well as the coordinate difference calculated from the data of [24–26]. The arrangement of Mo atoms in both models of structures is the same, the coordinates of heavy Ln atoms are close, while oxygen atoms deviate significantly from their centrosymmetric positions. The minimum deviations of the coordinates of oxygen atoms in space group $\bar{I}4c2$ from their positions in non-polar space group $I4_1/acd$ are observed for the Nd_2MoO_6 structure in comparison with similar values for the La_2MoO_6 and Pr_2MoO_6 structures (Table 2), which indicates that the high-temperature phase $I4_1/acd$ of the Nd_2MoO_6 single crystal is presumably fixed at room temperature.

Table 2. Atomic coordinates in the structure of Ln_2MoO_6 single crystals in space groups $I4_1/acd$ and $I\bar{4}c2$ and their difference Δ .

Atom	Ln	$I4_1/acd$			$I\bar{4}c2$			Δ		
		x/a	y/b	z/c	x/a	y/b	z/c	x/a	y/b	z/c
La1	La	0	0	0.16351(1)	0	0	0.16343(1)	0	0	0.00008
La1 ⁱ /La2		0.5	0	0.08649(1)	0.5	0	0.08639(1)	0	0	0.0001
Mo1		0.5	0	0.25	0.5	0	0.25	0	0	0
Mo1		0	0	0	0	0	0	0	0	0
Pr1	Pr	0	0	0.16311(1)	0	0	0.16318(1)	0	0	-0.00007
Pr1 ⁱ /Pr2		0.5	0	0.08689(1)	0.5	0	0.08698(1)	0	0	-0.00009
Mo1		0.5	0	0.25	0.5	0	0.25	0	0	0
Mo1 ⁱ /Mo2		0	0	0	0	0	0	0	0	0
Nd1	Nd	0	0	0.16294(1)	0	0	0.16323(1)	0	0	-0.00029
Nd1 ⁱ /Nd2		0.5	0	0.08706(1)	0.5	0	0.08734(1)	0	0	-0.00028
Mo1		0.5	0	0.25	0.5	0	0.25	0	0	0
Mo1 ⁱ /Mo2		0	0	0	0	0	0	0	0	0
O1	La	0.75	0.2409(2)	0.125	0.7443(1)	0.2411(1)	0.1249(1)	0.0057	-0.0002	0.0001
O2_1		0.3329(1)	0.1683(1)	0.2147(1)	0.3341(1)	0.1683(1)	0.2148(1)	-0.0012	0	-0.0001
O2_1 ⁱⁱ /O2_2		0.6683(1)	0.3329(1)	0.4647(1)	0.6682(1)	0.3312(1)	0.5353(1)	0.0001	0.017	-0.0706
O1	Pr	0.75	0.2669(3)	0.125	0.7322(1)	0.2459(6)	0.1255(1)	0.0178	0.021	-0.0005
O2_1		0.3355(1)	0.1758(1)	0.2143(1)	0.3322(1)	0.1691(3)	0.2871(1)	0.0033	0.0067	-0.0728
O2_1 ⁱⁱ /O2_2		0.6758(1)	0.3354(1)	0.4643(1)	0.6733(1)	0.3295(4)	0.4662(1)	0.0025	0.0059	-0.0019
O1	Nd	0.75	0.2567(1)	0.125	0.7524(1)	0.2567(1)	0.1249(1)	-0.0024	0	0.0001
O2_1		0.3348(1)	0.1757(1)	0.2859(1)	0.3314(1)	0.1679(1)	0.2859(1)	0.0034	0.0078	0
O2_1 ⁱⁱ /O2_2		0.6757(1)	0.1757(1)	0.5359(1)	0.6793(1)	0.3337(1)	0.5359(1)	-0.0036	0.0011	0

Symmetry operations of $I4_1/acd$ space group: (i) $-x + \frac{1}{2}, y, -z + \frac{1}{4}$; (ii) $y + \frac{1}{2}, x, z + \frac{1}{4}$. La2, Pr2, Nd2, Mo2, and O2_2 atoms correspond to $I\bar{4}c2$ space group. La1, Pr1, Nd1, Mo1, O1, and O2_1 atoms correspond to both space groups. The maximum displacements of oxygen atoms are highlighted in bold.

On the different Fourier maps of the electron density, peaks were found near the cation positions in the structure, which were not observed on the different Fourier maps of undoped Ln_2MoO_6 crystals. This allowed the authors of [24–26] to assume that such distribution of the residual electron density was associated with the incorporation of magnesium into the structure of the compounds. The presence of magnesium in the samples was additionally confirmed by scanning transmission electron microscopy and ICP-MS. Based on the data of electron microscopy, Mg cations were concluded to replace Mo cations in the structure. In the crystal structure of Ln_2MoO_6 oxymolybdates ($Ln = La, Pr, Nd$), impurity Mg atoms were localized near the positions of the Mo atoms Mo1 and Mo2 at a distance of ~ 0.3 Å. The peaks located on the difference Fourier maps near the Ln positions at distances of up to ~ 0.6 Å were interpreted as split positions of rare earth cations.

Structural models of the Ln_2MoO_6 ($Ln = La, Pr, Nd$) single crystals doped with Mg can be represented as superimposed lattices of the main matrix, Ln_2MoO_6 , (Figure 10) and lattices in which rare earth cation positions are split, and Mo cations are replaced by Mg. Since the Mg concentration in the crystal is low, there are few such lattices. The environment of the main cationic positions corresponds to the environment in the undoped Ln_2MoO_6 . The La, Pr, and Nd cations are located in the center of distorted cubes composed of O anions occupying the main positions; Mo atoms have a tetrahedral oxygen environment. The rare earth cations in the split positions are partially surrounded by oxygen atoms in the additional positions found. Surrounding the cations with oxygen anions located in low-occupancy positions leads to an even greater distortion of the shape of polyhedra in comparison with the undoped Ln_2MoO_6 . The doping Mg atoms in the structures are surrounded by eight O anions at distances of 2.1–2.9 Å, including two O atoms in additional positions. Thus, the partial replacement of Mo^{6+} with Mg^{2+} leads to disordering of O atoms,

decreasing in the occupancy of their positions and, as a consequence, to the appearance of oxygen vacancies in the structure of Mg-containing Ln_2MoO_6 oxymolybdates.

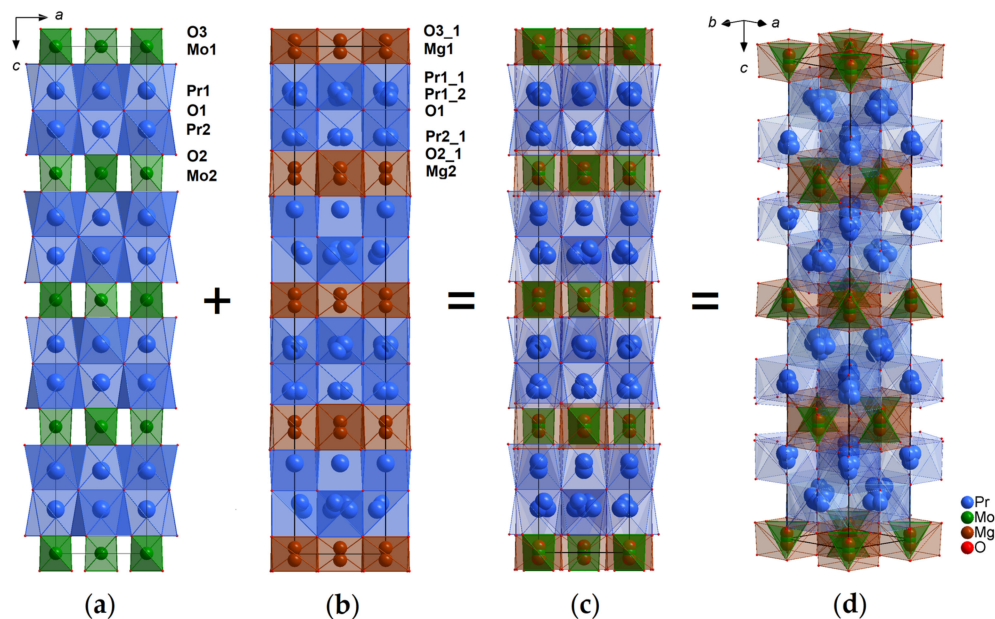


Figure 10. Model of the structure of Pr_2MoO_6 single crystals doped with magnesium: superimposed lattices of the (a) main matrix Pr_2MoO_6 ; (b) lattices in which Mg atoms are substituted for Mo atoms; (c,d) the resulting lattice in different projections [25] (Reproduced with permission of the International Union of Crystallography).

As shown above, significant weight loss on heating, as well as the corresponding absorption bands in the IR spectra, indicate the hygroscopic properties of Mg-doped oxymolybdates. It is known [35] that acceptor doping and the formation of oxygen vacancies in the structure leads to the dissolution of a significant amount of water from the gaseous atmosphere and the appearance of high-temperature proton conductivity as a functional property of the material. Consequently, there is a possibility of a proton component of the electrical conductivity of oxymolybdates of large rare earth metals with magnesium impurities in the structure.

4. Conclusions

Based on the analysis of the structures of single-crystal samples of Ln_2MoO_6 oxymolybdates ($Ln = La, Pr, Nd$), pure and doped with Mg, the motif of heavy atoms was found to be centrosymmetric in all compounds. The violation of the center of symmetry occurs due to displacements of the oxygen atoms surrounding the atoms of the rare earth element. Minimum deviations of the coordinates of oxygen atoms in space group $I\bar{4}c2$ from their positions in non-polar space group $I4_1/acd$ are observed for the Nd_2MoO_6 structure compared to La_2MoO_6 and Pr_2MoO_6 , which indicates that the high-temperature phase $I4_1/acd$ of the Nd_2MoO_6 single crystal is presumably fixed at room temperature. It should also be noted that among the three molybdates with the rare-earth cations La, Pr, and Nd, only the Nd_2MoO_6 compound at room temperature has a monoclinic scheelite-type structure, which at a temperature of about 1010 °C transforms into the tetragonal phase. Since the transition from the monoclinic phase to the high-temperature tetragonal phase is irreversible, tetragonal oxymolybdates synthesized at 1000 °C and higher temperatures are in a metastable state at room temperature. In all structures of Mg-doped single-crystal samples of oxymolybdates Ln_2MoO_6 ($Ln = La, Pr, Nd$), Mg cations were localized near the positions of Mo atoms, and the splitting of the positions of rare earth atoms was revealed.

The hygroscopic properties of the studied oxymolybdates were confirmed by thermogravimetry and IR spectroscopy. The incorporation of magnesium into the structure of oxymolybdates enhances the hygroscopic properties of the samples. Taking into account

the formation of oxygen vacancies in the structure upon partial substitution of Mg^{2+} atoms for Mo^{6+} , the proton component of the conductivity of oxymolybdates of large rare earth metals is probable.

Author Contributions: Synthesis of polycrystalline samples and IR spectroscopy, writing—original draft preparation, E.O.; TG and DSC analysis; analysis, validation, E.K.; X-ray phase analysis, T.S.; X-ray diffraction analysis, visualization, A.A.; X-ray diffraction analysis, visualization, translation, data curation, N.N.; X-ray diffraction analysis, writing—original draft preparation, supervision, N.S.; crystal growth by the flux method, writing—original draft preparation, as well as review and editing, project administration, V.V. All authors have read and agreed to the published version of the manuscript.

Funding: The following funding is acknowledged: Russian Foundation for Basic Research (award No. 18-29-12005). This work was performed using the equipment of the Shared Research Center FSRC “Crystallography and Photonics” RAS and was supported by the Ministry of Science and Higher Education of the Russian Federation within the State assignment FSRC “Crystallography and Photonics” RAS with respect to the X-ray phase and structure analyses and by the Russian Foundation for Basic Research with respect to the synthesis of the crystals and the study of their thermogravimetric and spectroscopic properties.

Institutional Review Board Statement: Expert opinion No. 681 of 21 May 2021 on the possibility of open publication and Permission No. 681 of 24 May 2021 for the export or dispatch of material abroad.

Informed Consent Statement: Informed consent was obtained from all subjects involved in the study.

Data Availability Statement: The structural data are deposited with the Cambridge Crystallographic Data Centre. CCDC references: 1999199; 1999200; 2086342.

Acknowledgments: The authors are grateful to A.L. Vasiliev for his help in obtaining the data of scanning electron microscopy.

Conflicts of Interest: The authors declare no conflict of interest.

References

1. Blasse, G. Dlanthanide molybdate and tungstates Ln_2MoO_6 . *J. Inorg. Nucl. Chem.* **1966**, *28*, 1488–1489. [CrossRef]
2. Pokrovskii, A.N.; Rybakov, V.K.; Trunov, V.K. XRD study of oxytungstate and oxymolybdate of lanthanides and ittrium oxymolybdate. *Zhurnal Neorg. Khimii* **1969**, *14*, 2344–2347.
3. McCarthy, G.J.; Fischer, R.D.; Johnson, G.G., Jr.; Gooden, C.E. Crystal Chemistry and Compound Formation in the Systems Rare Earth Sesquioxide— WO_3 . In Proceedings of the Fifth Material Research Symposium on Solid State Chemistry, Gaithersburg, MD, USA, 18 October 1971; pp. 397–411. Available online: https://inis.iaea.org/search/search.aspx?orig_q=RN:4068137 (accessed on 27 May 2021).
4. Brixner, L.N.; Sleight, A.W.; Lics, M.S. La_2MoO_6 —Type rare earth molybdates—Preparation and lattice parameters. *J. Solid State Chem.* **1972**, *5*, 186–190. [CrossRef]
5. Dorn, K.V.; Hartenbach, I. Press to success: $Gd_5FW_3O_{16}$ —The first gadolinium(III) fluoride oxidotungstate(VI). *Crystals* **2019**, *9*, 424. [CrossRef]
6. Errandonea, D.; Ruiz-Fuertes, J. A brief review of the effects of pressure on wolframite-type oxides. *Crystals* **2018**, *8*, 71. [CrossRef]
7. Nassau, K.; Levinstein, H.J.; Loiacono, G.M. A comprehensive study of trivalent tungstates and molybdates of the type $L_2(MO_4)_3$. *J. Phys. Chem. Solids* **1965**, *26*, 1805–1816. [CrossRef]
8. Lacorre, P.; Goutenoire, F.; Bohnke, O.; Retoux, R.; Laligant, Y. Designing fast oxide-ion conductors based on $La_2Mo_2O_9$. *Nat. Cell Biol.* **2000**, *404*, 856–858. [CrossRef] [PubMed]
9. Hubert, P.H.; Michel, P.; Thozet, A. Structure of neodymium molybdenite $Nd_5Mo_3O_{16}$. *C. R. Hebd. Seances Acad. Sci. Ser. C* **1973**, *276*, 1779–1781.
10. Meng, F.; Zhang, X.; Li, H.; Seo, H.J. Synthesis and spectral characteristics of $La_2MoO_6 \cdot Ln^{3+}$ ($Ln = Eu, Sm, Dy, Pr, Tb$) polycrystals. *J. Rare Earths* **2012**, *30*, 866–870. [CrossRef]
11. Colmont, M.; Boutinaud, P.; Latouche, C.; Massuyeau, F.; Huvé, M.; Zadoya, A.; Jobic, S. Origin of luminescence in La_2MoO_6 and $La_2Mo_2O_9$ and their Bi-doped variants. *Inorg. Chem.* **2020**, *59*, 3215–3220. [CrossRef]
12. Chen, Y.C.; Weng, M.Z. Improving quality factor of Nd_2MoO_6 ceramics by removing moisture content. *J. Mater. Sci. Mater. Electron.* **2015**, *26*, 3502–3505. [CrossRef]
13. Hu, S.; Zhou, H.; Zhou, H.; Luan, X.; Wang, K.; Chen, X. Phase structure, sintering behaviour and microwave dielectric properties of Ln_2MoO_6 ($Ln = La$ and Y) ceramics. *Ceram. Int.* **2020**, *46*, 24552–24556. [CrossRef]
14. Sillen, L.G.; Lundburg, K. La_2MoO_6 , ein Lanthanoxymolybdat mit Schichtenstruktur. *Z. Anorg. Chem.* **1943**, *252*, 2–8. [CrossRef]

15. Klevtsov, P.V.; Khartchenko, L.Y.; Klevtsova, R.F. Crystallization and polymorphism of rare-earth oxymolybdates of composition Ln_2MoO_6 . *Kristallografiya* **1975**, *20*, 571–578.
16. Efremov, V.A.; Tyulin, A.V.; Trunov, V.K. Actual structure of tetragonal $\text{Ln}_2\text{O}_2\text{MoO}_4$ and factors, determining the distortion of structure—Forming coordination polyhedral. *Koord. Khim.* **1987**, *13*, 1276–1282.
17. Xue, J.S.; Antonio, M.R.; Soderholm, L. Polymorphs of Ln_2MoO_6 : A neutron diffraction of the crystal structures of La_2MoO_6 and Tb_2MoO_6 . *Chem. Mater.* **1995**, *7*, 333–340. [[CrossRef](#)]
18. Polyanskaya, T.M.; Borisov, S.V.; Belov, N.V. A new form of the sheelite structural type: Crystal structure of Nd_2WO_6 . *Dokl. Akad. Nauk SSSR* **1970**, *193*, 83–86.
19. Evdokimov, A.A.; Efremov, V.A.; Trunov, V.K.; Kleinman, I.A.; Dzhurinskyi, B.Ph. *Rare-Earth Compounds. Molybdates and Tungstates*; Nauka: Moscow, Russia, 1991.
20. Antipin, A.M.; Sorokina, N.I.; Alekseeva, O.A.; Dudka, A.P.; Chernyshev, D.Y.; Voronkova, V.I. Polymorphism and structure of Nd_2MoO_6 single crystals. *Crystallogr. Rep.* **2017**, *62*, 537–544. [[CrossRef](#)]
21. Voronkova, V.; Orlova, E.; Kazakov, S.; Kharitonova, E.; Belov, D. Phase relations and physical properties of layered Pb-containing Nd_2MoO_6 compounds. *Eur. J. Inorg. Chem.* **2016**, *2016*, 1022–1029. [[CrossRef](#)]
22. Kuzmicheva, G.M. *Main Crystal Chemical Categories*; MITHT: Moscow, Russia, 2001.
23. Yanovskii, V.K.; Voronkova, V.I. Electroconductivity of tungstates and molybdates of A_2BO_6 and Meyer–Neldel rule. *Solid State Physics.* **1977**, *19*, 3318–3321.
24. Voronkova, V.I.; Kharitonova, E.P.; Orlova, E.I.; Sorokina, N.I.; Sorokin, T.A.; Antipin, A.M.; Baldin, E.D.; Grebenev, V.V. Synthesis, structure, and physical properties of layered tetragonal Mg-doped Nd_2MoO_6 compounds. *J. Alloy. Compd.* **2019**, *803*, 1045–1053. [[CrossRef](#)]
25. Voronkova, V.I.; Antipin, A.M.; Sorokin, T.A.; Novikova, N.E.; Kharitonova, E.P.; Orlova, E.I.; Kvartalov, V.B.; Presniakov, M.Y.; Bondarenko, V.I.; Vasiliev, A.L.; et al. Synthesis, structure and properties of layered Pr_2MoO_6 -based oxymolybdates doped with Mg. *Acta Crystallogr. Sect. B Struct. Sci. Cryst. Eng. Mater.* **2020**, *76*, 492–501. [[CrossRef](#)]
26. Orlova, E.I.; Kharitonova, E.P.; Sorokina, N.I.; Sorokin, T.A.; Antipin, A.M.; Voronkova, V.I. Structure and physical properties of Mg-containing oxymolybdates La_2MoO_6 . *Crystallogr. Rep.* **2020**, *65*, 697–703. [[CrossRef](#)]
27. Voronkova, V.; Kharitonova, E.; Orlova, E.; Gorshkov, N.; Goffman, V. Synthesis and unusual properties of tetragonal Pb-containing oxymolybdates based on La_2MoO_6 . *Eur. J. Inorg. Chem.* **2017**, *2017*, 5582–5587. [[CrossRef](#)]
28. Rigaku Oxford Diffraction. *CrysAlisPro Software System, Version 1.171.39.46*; Rigaku Corporation: Oxford, UK, 2018.
29. Clark, R.C.; Reid, J.S. The analytical calculation of absorption in multifaceted crystals. *Acta Crystallogr. Sect. A Found. Crystallogr.* **1995**, *51*, 887–897. [[CrossRef](#)]
30. Petříček, V.; Dušek, M.; Palatinus, L. Crystallographic computing system JANA2006: General features. *Z. Kristallogr.* **2014**, *229*, 345–352. [[CrossRef](#)]
31. Palatinus, L. Ab initio determination of incommensurately modulated structures by charge flipping in superspace. *Acta Crystallogr.* **2004**, *60*, 604–610. [[CrossRef](#)]
32. Colomban, P. Proton and protonic species: The hidden face of solid state chemistry. How to measure H-content in materials? *Fuel Cells* **2012**, *13*, 6–18. [[CrossRef](#)]
33. Fomichev, V.V.; Kondratov, O.I.; Gagarin, V.A.; Gokhman, L.Z.; Petrov, K.I. Investigation of vibrational spectra of oxymolybdates of rare earth elements. *Zhurnal Neorganicheskoy Khimii* **1977**, *22*, 2150–2157.
34. Yukhnovich, G.V. *Infrared Spectroscopy of Water*; Nauka: Moscow, Russia, 1973.
35. Animitsa, I.E. Proton Transport. In *Complex. Oxides. Tutorial*; Ural University Publishing House: Ekaterinburg, Russia, 2014.